POLITECNICO DI TORINO
Repository ISTITUZIONALE

A correlation noise spectrometer for flicker noise measurement in graphene samples

Original
A correlation noise spectrometer for flicker noise measurement in graphene samples / Marzano, Martina; Cultrera, Alessandro; Ortolano, Massimo; Callegaro, Luca. - In: MEASUREMENT SCIENCE & TECHNOLOGY. - ISSN 0957-0233. - STAMPA. - 30:3(2019), p. 035102. [10.1088/1361-6501/aafcab]

Availability:
This version is available at: 11583/2724902 since: 2019-02-10T12:58:15Z

Publisher:
IOP

Published
DOI:10.1088/1361-6501/aafcab

Terms of use:

This article is made available under terms and conditions as specified in the corresponding bibliographic description in the repository

Publisher copyright
IOP postprint/Author's Accepted Manuscript

“This is the accepted manuscript version of an article accepted for publication in MEASUREMENT SCIENCE & TECHNOLOGY. IOP Publishing Ltd is not responsible for any errors or omissions in this version of the manuscript or any version derived from it. The Version of Record is available online at http://dx.doi.org/10.1088/1361-6501/aafcab

(Article begins on next page)

27 April 2026

A correlation noise spectrometer for flicker noise measurement in graphene samples

Martina Marzano[1,2], Alessandro Cultrera[2], Massimo Ortolano[1,2], Luca Callegaro[2]

[1] Politecnico di Torino, Dipartimento di Elettronica e Informazione, Corso Duca degli Abruzzi 24, 10129 Torino, Italy

[2] INRIM — Istituto Nazionale di Ricerca Metrologica, Strada delle Cacce 91, 10135 Torino, Italy

E-mail: `martina.marzano@polito.it`

October 2018

Abstract. We present a high-resolution digital correlation spectrum analyzer for the measurement of low frequency resistance fluctuations in graphene samples. The system exploits the cross-correlation method to reject the amplifiers' noise. The graphene sample is excited with a low-noise DC current. The output voltage is fed to two two-stage low-noise amplifiers connected in parallel; the DC signal component is filtered by a high-pass filter with a cutoff frequency of 34 mHz. The amplified signals are digitized by a 2-channel synchronous ADC board; the cross-periodogram, which rejects uncorrelated amplifiers' noise components, is computed in real time. As a practical example, we measured the noise cross-spectrum of graphene samples in the frequency range from 0.153 Hz to 10 kHz, both in 2- and 4-wire configurations, and for different bias currents. We report here the measurement setup, the data analysis and the error sources.

Submitted to: *Meas. Sci. Technol.*

1. Introduction

Like other electrically conducting materials, when crossed by a current, graphene exhibits electrical *excess noise*, dominated by flicker ($1/f$) noise. Flicker noise limits the resolution of sensors [1–4] and the sensitivity of amplifiers and detectors [5–7]. Moreover, in recent years, several works proposed graphene sensors based on electrical noise output [7–10].

Flicker noise in graphene is highly dependent on the growth technique, the device fabrication technology and the specific bias conditions [5, 11–17]. A proper characterisation of magnitude and spectral properties of flicker noise is essential to enable its adoption as an industrial material for future electronics.

The accurate measurement of flicker noise spectral density is made difficult by the small magnitude of the signal to be measured (in the $\mathrm{nV\,Hz^{-1/2}}$ range) [18], and the long measurement time required to probe the low frequency region [19].

A direct measurement using a single-channel signal analyzer is corrupted by the flicker noise of the instrument itself [20–22], which can have a magnitude comparable to that of the signal of interest. A correction can be performed, but requires an independent measurement of the noise floor [23, 24]. Interferences, often from mains, are another typical source of error.

The experimental design must take into consideration the DC voltage caused by the device bias current, which can overload a DC-coupled instrument input stage. AC coupling in commercial amplifiers is available, but typically with a cutoff frequency of tenths of hertz (see e.g. [25]), causing significant errors on measurements performed below 10 Hz.

This paper presents a digital correlation spectrum analyzer for the measurement of flicker noise of graphene samples.

The analyzer is based on cross-correlation [26, 27], which rejects to a large extent the noise of the amplifiers, and thus allows to determine the device noise power spectrum under DC current excitation. Both analogue [28, 29] and digital [30, 31] cross-correlators have been described in the literature, the most accurate implementations being employed in Johnson noise thermometry experiments [32–34]. Although not perfect [35–37], the rejection of amplifiers' noise given by correlation is particularly effective at low frequency, and therefore in flicker noise measurements.

The analyzer here described is based on a two-channel voltage signal conditioning system, including low-noise, high-gain amplifiers and a synchronous sampling system. The acquired samples are processed by a digital correlation algorithm. At variance with commercial signal analyzers (see e.g. [25] and [38]), the lowest measurement frequency can be virtually arbitrarily extended, with a number of frequency points up to 2^{17}. Proper wiring and shielding reduce interferences to negligible levels.

In section 4, examples of flicker noise measurements on graphene samples are shown.

2. Noise measurement concepts

2.1. Basics of cross-correlation

Noise measurements on devices require the amplification of small signals. Amplifiers, however, introduce additional noise components. The cross-correlation method rejects the amplifiers' noise by simultaneously amplifying the device noise with two different amplifiers and by combining their output signals in a suitable way.

Let us briefly review the cross-correlation

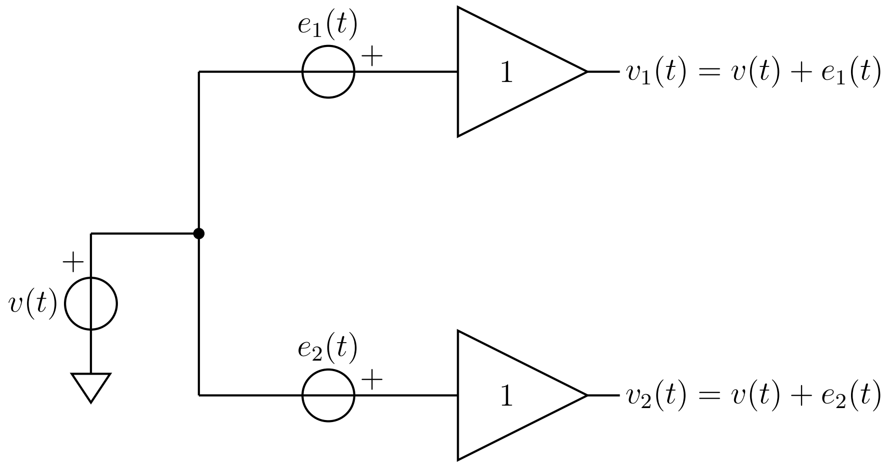

Figure 1: Equivalent circuit of a spectrum analyzer based on the cross-correlation method.

method by referring to the principle schematic of figure 1: $v(t)$ represents the device noise signal, which is the quantity of interest; $e_1(t)$ and $e_2(t)$ are the amplifiers' noise components; the amplifier gains are assumed to be 1, without loss of generality. We assume that the signals are realizations of stationary and ergodic random processes. For this class of processes, the main statistical properties are described by the auto- and cross-correlation functions or, equivalently, in the frequency domain, by the spectral density and cross-spectral density functions (or, respectively, spectrum and cross-spectrum).

The signals $v_1(t)$ and $v_2(t)$ at the amplifiers' outputs are

$$v_1(t) = v(t) + e_1(t), \tag{1}$$

$$v_2(t) = v(t) + e_2(t). \tag{2}$$

We assume that $v(t)$, $e_1(t)$ and $e_2(t)$ are uncorrelated, that is, for all time lags τ,

$$\mathrm{E}\{e_1(t)e_2(t+\tau)\} = 0, \tag{3}$$

$$\mathrm{E}\{v(t)e_i(t+\tau)\} = 0, \qquad i = 1, 2, \tag{4}$$

where $\mathrm{E}\{\cdot\}$ denotes the expected value of the argument. With these assumptions, the cross-correlation of $v_1(t)$ and $v_2(t)$ is

$$\begin{aligned} R_{12}(\tau) &= \mathrm{E}\{v_1(t)v_2(t+\tau)\}, \\ &= \mathrm{E}\{[v(t) + e_1(t)][v(t+\tau) + e_2(t+\tau)]\}, \\ &= \mathrm{E}\{v(t)v(t+\tau)\} + 0, \\ &= R_{vv}(\tau), \end{aligned} \tag{5}$$

which coincides with the auto-correlation function $R_{vv}(\tau)$ of the device noise. The terms depending on the uncorrelated noise components are thus rejected: there only remains the term depending on the correlated noise at the amplifiers' inputs.

Equivalently, in the frequency domain, the cross-spectrum, which is defined as the Fourier transform of the cross-correlation $R_{12}(\tau)$, coincides with the spectrum $S_v(f)$ of the only correlated component. In fact, from (5),

$$\begin{aligned} S_{12}(f) &= \int_{-\infty}^{\infty} R_{12}(\tau)\mathrm{e}^{-\mathrm{j}2\pi f\tau}\,\mathrm{d}\tau, \\ &= \int_{-\infty}^{\infty} R_{vv}(\tau)\mathrm{e}^{-\mathrm{j}2\pi f\tau}\,\mathrm{d}\tau = S_v(f). \end{aligned} \tag{6}$$

Typically, to estimate $S_{12}(f)$ and $S_v(f)$, the signals $v_1(t)$ and $v_2(t)$ are periodically and simultaneously sampled and acquired with sampling period T_s. We denote the N acquired samples by $v_1[n]$ and $v_2[n]$, $n = 1, \ldots, N$.

We choose the cross-periodogram [39, section 9.5] as an estimator of the cross-spectrum and to reduce the uncertainty we

adopt the Bartlett lag window [40, section 6.2]. Let us consider NM samples splitted into M groups of N samples each; the cross-periodogram associated to group m, $m = 1, \dots, M$, is

$$\hat{S}^{(\mathrm{p})}_{12,m}(f_k) = \\ = \frac{T_\mathrm{s}}{N} \left\{ \sum_{n=1}^{N} v_1[(m-1)N + n] \mathrm{e}^{-\mathrm{j}2\pi f_k n T_\mathrm{s}} \right\}^* \\ \times \left\{ \sum_{n'=1}^{N} v_2[(m-1)N + n'] \mathrm{e}^{-\mathrm{j}2\pi f_k n' T_\mathrm{s}} \right\}, \quad (7)$$

where $f_k = k/(NT_\mathrm{s})$, $k = 0, \dots, N-1$, are the Fourier frequencies and the asterisk denotes complex conjugation. The reciprocal of the acquisition time $T_0 = NT_\mathrm{s}$ corresponds to the resolution bandwidth. The average value of the M periodograms,

$$\hat{S}_{12}(f_k) = \frac{1}{M} \sum_{m=1}^{M} \hat{S}^{(\mathrm{p})}_{12,m}(f_k), \quad (8)$$

is an estimator of $S_{12}(f)$ whose variance [39, section 9.5]

$$\mathrm{var}\{\hat{S}_{12}(f_k)\} \sim \frac{1}{M} S_{v_1}(f_k) S_{v_2}(f_k) \quad (9)$$

depends on M and on the power spectral densities of the signals $v_1(t)$ and $v_2(t)$,

$$S_{v_j}(f_k) = S_v(f_k) + S_{e_j}(f_k) \qquad j = 1, 2. \quad (10)$$

The uncertainty of this estimator thus depends on the amplifiers' noise, and choosing a sufficiently large M allows to reduce the uncertainty to the desired level.

2.2. Systematic error sources

A detailed analysis of the error sources in the cross-correlation method can be found in [36, 37, 41]. Here we briefly summarize the results in a form suitable to estimate the systematic error of the setup described in section 3.

A simplified equivalent circuit for the error analysis is shown in figure 2. The device is represented by a Thévenin's equivalent circuit composed of the noise signal source $v(t)$ in series with the resistance R. The two amplifiers have equal gain, which we assume to be 1, and equal input impedance $Z_\mathrm{i}(f)$. The amplifiers' output voltages are $v_1(t)$ and $v_2(t)$. The voltage sources $e_1(t)$ and $e_2(t)$ represent the equivalent input noise voltage of the amplifiers; the current sources $j_1(t)$ and $j_2(t)$ represent the input *short-circuit* noise current of the amplifiers‡.

The currents $j_1(t)$ and $j_2(t)$, crossing R and the impedances Z_i, generate a voltage which adds to the signal of interest, thus causing a systematic error in the estimation of $S_v(f)$. Following [37], it can be shown that the systematic error $\Delta S_v(f)$ on $S_v(f)$ is given by

$$\Delta S_v(f) = R^2 [S_{j_1}(f) + S_{j_2}(f)] \\ - R \frac{\mathrm{Re}[A(f) S^*_{e_1 j_1}(f) + A(f) S^*_{e_2 j_2}(f)]}{|A(f)|^2}, \quad (11)$$

where $S_{j_1}(f)$ and $S_{j_2}(f)$ are, respectively, the spectral density functions of $j_1(t)$ and $j_2(t)$, $S_{e_1 j_1}(f)$ and $S_{e_2 j_2}(f)$ are, respectively, the cross-spectral density functions between $e_1(t)$ and $j_1(t)$ and between $e_2(t)$ and $j_2(t)$,

$$A(f) = \frac{1}{1 + 2R/Z_\mathrm{i}(f)} \quad (12)$$

is the input attenuation, and the operator Re takes the real part of the argument.

At low frequency, capacitive effects are negligible and the input impedance is usually very high. As a consequence, $|A(f)| \approx 1$ and the contribution of the voltage noise to $S_{j_1}(f)$ and $S_{j_2}(f)$ is usually negligible (see also [37]). The cross-spectra $S_{e_1 j_1}(f)$ and $S_{e_2 j_2}(f)$ are

‡ The short-circuit noise current contains also the current injected by the noise voltage through the finite input impedance: with this choice, the input impedance Z_i can be moved upstream of the noise voltage sources, and the equation can be simplified.

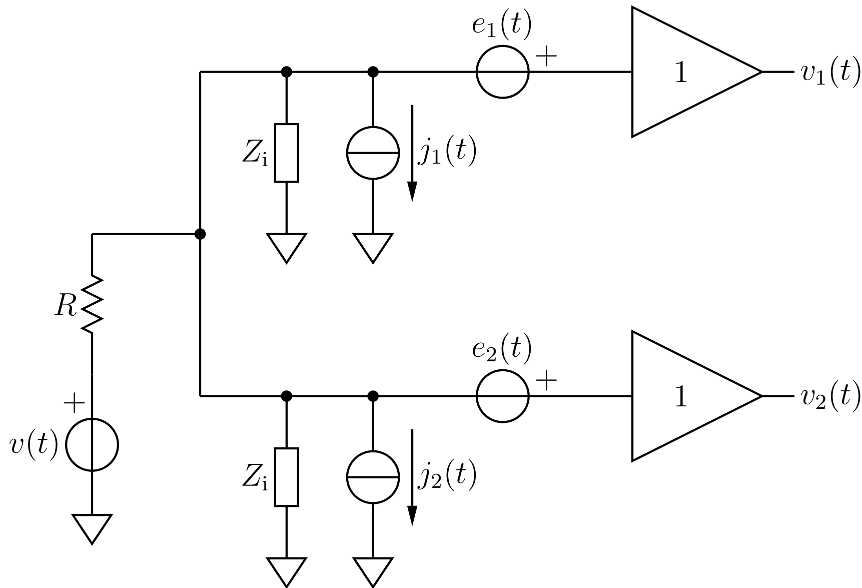

Figure 2: Equivalent circuit for the analysis of systematic errors.

of difficult evaluation, but at low frequency their contribution is usually negligible too. Taking into account these conditions, we shall approximate the error at low frequency as

$$\Delta S_v(f) \approx R^2[S_{j_1}(f) + S_{j_2}(f)]. \qquad (13)$$

3. Measurement setup

The voltage noise of a device or a circuit can be measured with a digital correlation spectrum analyzer in a shielded and temperature controlled environment. Here the device is a graphene sample in the form of a Hall bar. If the sample is unbiased, the measured signal includes only the thermal, white noise component. Instead, if the sample is crossed by a DC bias current, both white and excess noise components are measured.

The measurement setup, as shown diagrammatically in figure 3, is composed of a test circuit, amplifiers and a data acquisition board. Here we describe the setup in a 2-terminal configuration; the extension to the 4-terminal configuration is straightforward.

The test circuit, represented in figure 4, allows to measure the noise signal $v(t)$ of the sample with or without a DC bias current, which can be turned on and off by the switch S. The bias current is generated by the voltage source E in series with the $10\,\mathrm{M\Omega}$ metal resistor R_B, having negligible excess noise. The voltage source E consists of four series-connected 1.2 V NiCd batteries and a dip switch allowing to set E to 1.2 V, 2.4 V, 3.6 V or 4.8 V. The two outputs, 1 and 2, are AC coupled by two high-pass filters with a cutoff frequency of 34 mHz. The test circuit is shielded by a box connected to the low terminal of the battery.

The noise signal $v(t)$ at the outputs 1 and 2 is then amplified simultaneously by two two-stage low noise amplifiers with a total gain of 10^4 (figure 3). The first stage is composed of two battery-powered commercial amplifiers with a gain of 100: an EG&G PAR 113 pre-amplifier ($10\,\mathrm{nV\,Hz^{-1/2}}$ nominal voltage noise, $7\,\mathrm{fA\,Hz^{-1/2}}$ current noise at 1 kHz) and an EG&G PAR 5113 pre-amplifier ($4\,\mathrm{nV\,Hz^{-1/2}}$ nominal voltage noise, $40\,\mathrm{fA\,Hz^{-1/2}}$ current

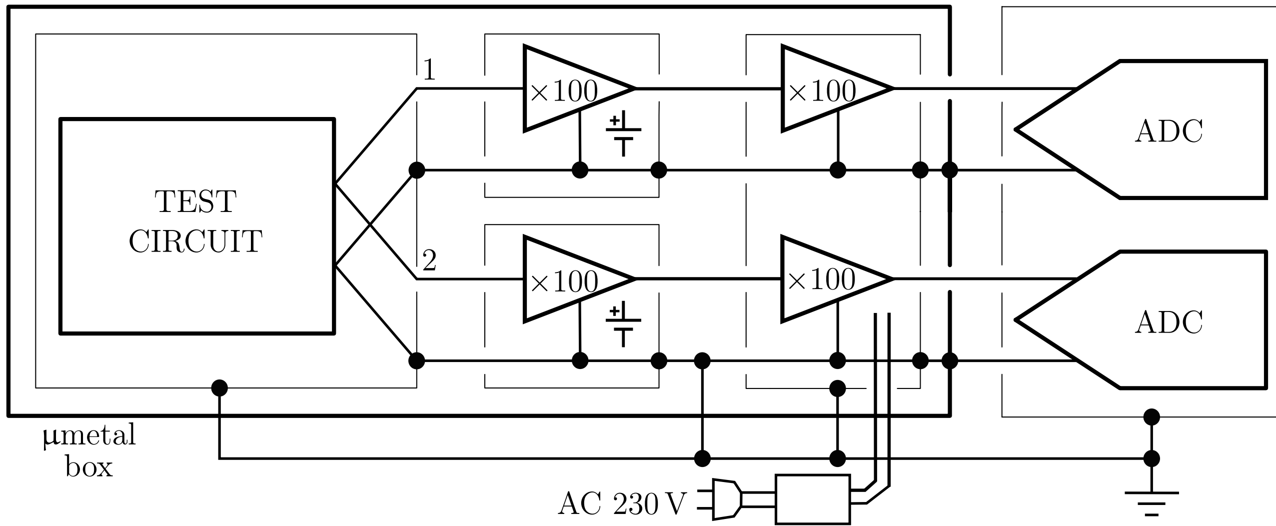

Figure 3: Block schematic of the digital correlation spectrum analyzer, composed of a test circuit, amplifiers and data acquisition board with analogue-to-digital converters. The test circuit and the amplifiers are individually electrically shieldied (thin rectangles) and further magnetically shieldied by a µmetal box (thick rectangle).

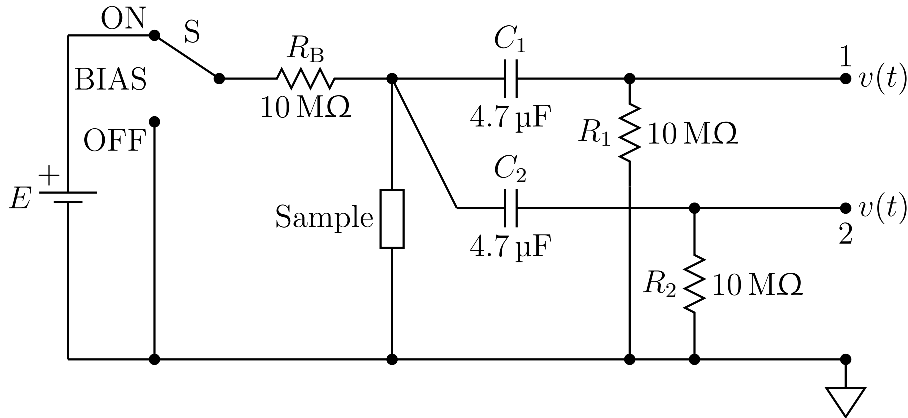

Figure 4: Schematic of the test circuit.

noise at 1 kHz). The second stage is composed of two bespoke amplifiers with a gain of 100 ($10\,\mathrm{nV\,Hz^{-1/2}}$ voltage noise), powered by a dedicated regulated power supply.

The test circuit (figure 5(a)) and the two two-stage amplifiers are contained in an electrically and magnetically shielded µmetal box, as shown in figure 5(b). The amplifiers' outputs are connected to a PXI rack, equipped with the data acquisition board (National Instruments 4462) that communicates through an optical fiber with a computer. The board is characterized by a resolution of 24 bit and a maximum sampling frequency of 204.8 kHz. A software controls the signal acquisition. A typical measurement is composed of $N = 2^{17}$ pairs of samples acquired at a sampling rate of 20 kHz. The resolution bandwidth is 0.153 Hz and the duration T_0 of a single acquisition is of about 6.5 s. The shielded boxes and the

amplifiers have the same ground connected to the PXI external ground.

4. Example measurements on graphene samples

As an example application of the setup described in section 3, we present a series of noise measurements on two graphene samples, labeled respectively AEM23C and AEM22A (see [17] for an in-depth analysis of the measurements). The Hall bars were fabricated from commercial chemical vapor deposited monolayer graphene. The geometry was defined by means of electron beam lithography and oxygen plasma etching. Cr/Au electrodes were deposited with an electron-gun evaporator. Figure 6(a) shows a scanning electron microscope image of the sample AEM23C.

Noise measurements were performed in 2- and 4-terminal configurations (see figures 6(b) and 6(c)), and at different bias current levels. The 2-terminal configuration corresponds to the schematic of figure 4.

Figure 7(a) shows the successful rejection of uncorrelated noise by the cross-correlation technique. In this figure, three voltage noise spectra from sample AEM23C are reported. The two spectra labelled $\hat{S}_{v_1}(f)$ and $\hat{S}_{v_2}(f)$ were measured in the 2-terminal configuration with no bias current and represent the measurements at the two amplifiers' outputs (scaled by the gain). The spectrum labelled $\hat{S}_{12}(f)$ is the estimated cross-spectrum of $\hat{S}_{v_1}(f)$ and $\hat{S}_{v_2}(f)$. All the estimated spectra were obtained by averaging $M = 250$ periodograms. The spectra $\hat{S}_{v_1}(f)$ and $\hat{S}_{v_2}(f)$ contain the thermal noise from the unbiased sample but also the amplifiers' noise, with $1/f$ components. These components are uncorrelated and are rejected in the cross-spectrum $\hat{S}_{12}(f)$ as expected from (5).

Figure 7(b) reports four cross-spectra, obtained in both 2-terminal (2T) and 4-terminal (4T) configurations and with (on) or without (off) bias current. The cross-spectra from the unbiased sample consist of the thermal noise component only; the thermal noise level measured in 2- and 4-terminal configurations is the same because the equivalent resistance of the sample as seen from the voltage terminals is the same in both configurations (figure 6). Instead, the cross-spectra from the biased sample contain also a $1/f$ noise component, and the $1/f$ noise level in the 2-terminal configuration is one order of magnitude greater than that in the 4-terminal configuration. This ratio is due to the fact that in the 2-terminal configuration the bias current crosses the c-shaped graphene segment (dashed line in figure 6(b)) and the contacts, whereas in the 4-terminal configuration the bias current crosses only the center bar of the sample (dashed line in figure 6(c)) and only a fraction of the generated $1/f$ noise is thus measured. Given the sample geometry and the bias current paths, if the excess noise were generated in the graphene only, there would have been a ratio of about 3 between the $1/f$ noise levels measured in 2- and 4-terminal configurations. The extra factor can be ascribed to the contacts [17].

The systematic error due to the amplifiers' input currents can be estimated from (13) and from the amplifiers' current noise specifications reported in section 3. It is worth noting that for FET-input amplifiers, like those chosen for this experiment, the current noises $S_{j_1}(f)$ and $S_{j_2}(f)$ are white down to very low frequency, and this implies that the systematic error is constant also in the flicker noise region of interest. For a resistance of the order of $10\,\mathrm{k\Omega}$, $\Delta S_v(f) \approx 1.6 \times 10^{-19}\,\mathrm{V^2\,Hz^{-1}}$, independent of

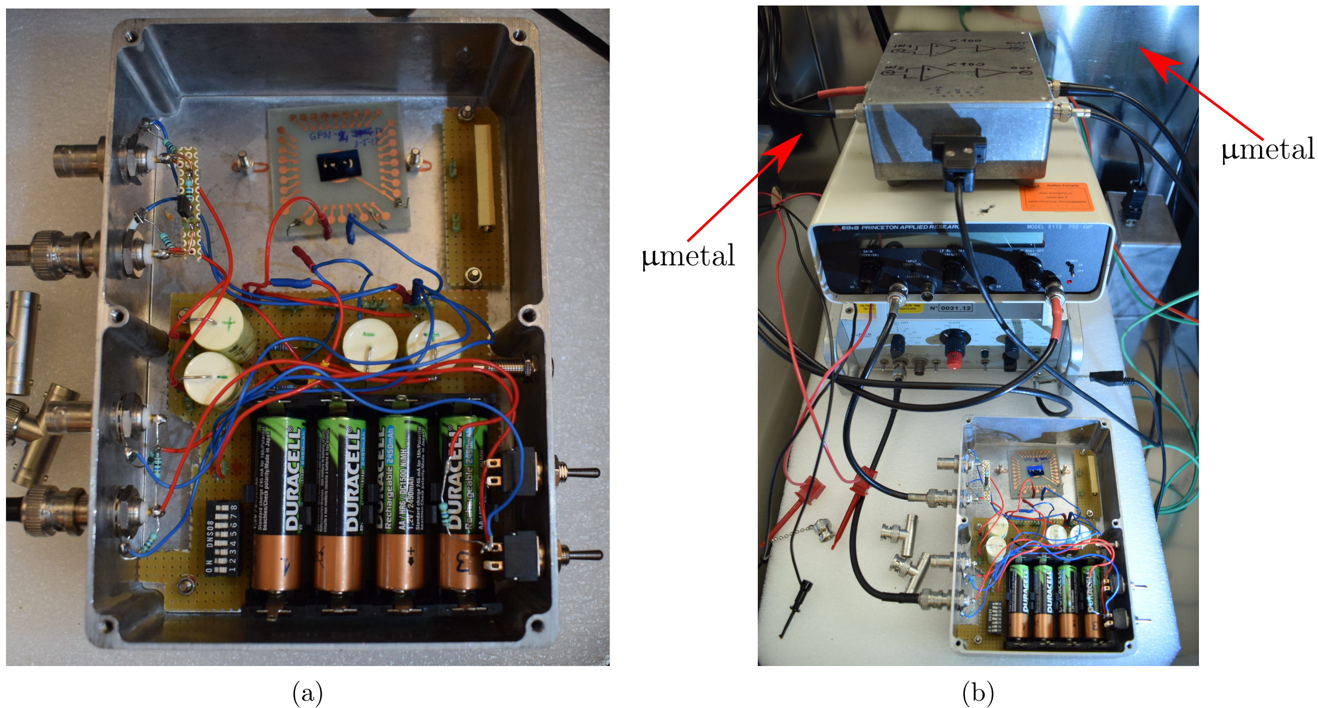

(a) (b)

Figure 5: Measurement setup: (a) test circuit placed in an electrically shielding box (top cover removed); (b) test circuit and two-stage amplifiers placed in a large magnetically shielding µmetal box (top cover removed).

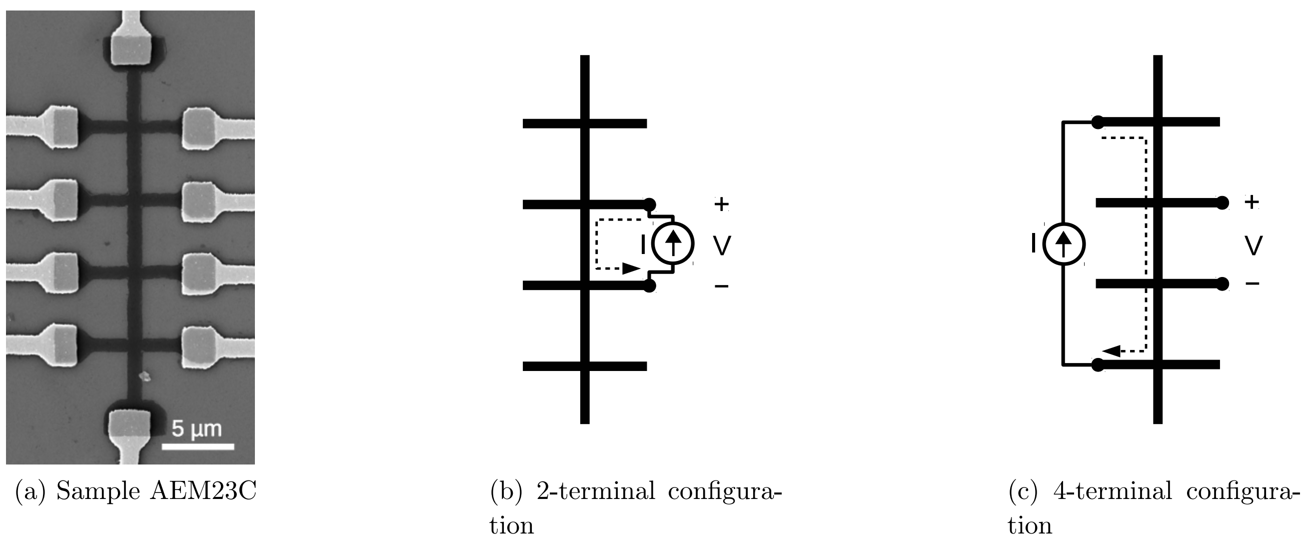

(a) Sample AEM23C (b) 2-terminal configuration (c) 4-terminal configuration

Figure 6: (a) Scanning electron microscope image of the graphene Hall bar AEM23C; (b) 2-terminal measurement configuration: the noise voltage $v(t)$ is measured across the same terminals at which the DC bias current I is applied; (c) 4-terminal measurement configuration: the noise voltage is measured across two terminals which are different from those at which the DC bias current is applied. The dashed lines represent the bias current path in the respective cases.

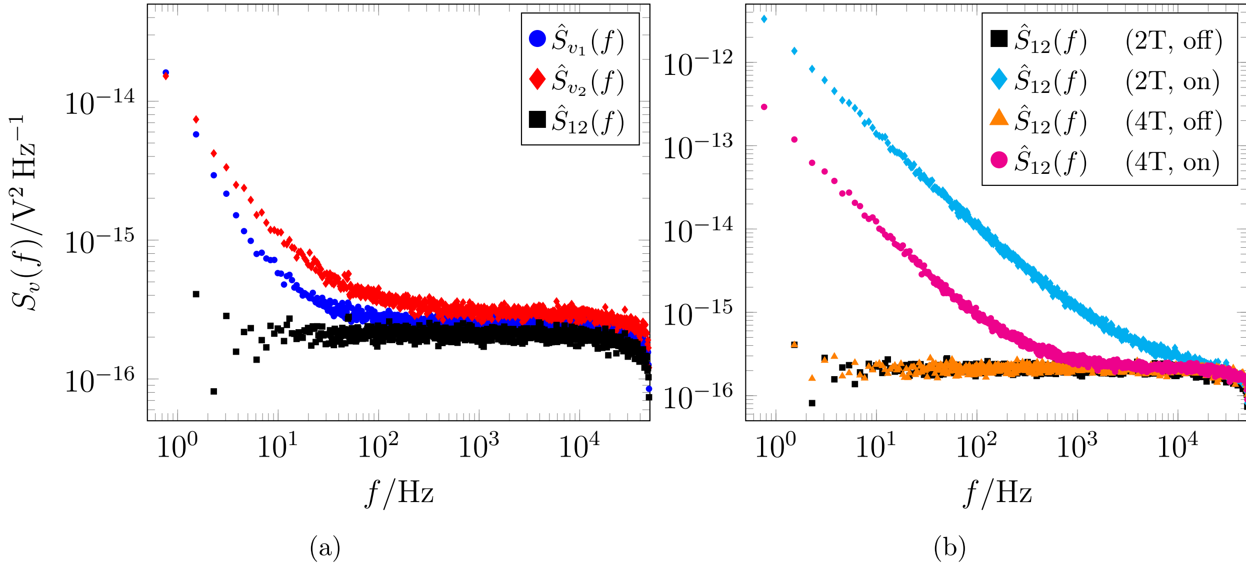

Figure 7: Voltage noise spectra of sample AEM23C in different measurement configurations: (a) estimated spectra $\hat{S}_{v_1}(f)$ and $\hat{S}_{v_2}(f)$ measured in 2-terminal configuration without bias and the corresponding cross-spectrum $\hat{S}_{12}(f)$; (b) comparison between 2-terminal (2T) and 4-terminal (4T) configurations with (on) or without (off) DC bias current.

frequency. The type A uncertainty associated to the spectra can be evaluated from (9). For instance, from figure 7(a),

$$\hat{S}_{v_1}(f) \approx 2 \times 10^{-16}\,\mathrm{V}^2\,\mathrm{Hz}^{-1} \times \left(1 + \frac{20\,\mathrm{Hz}}{f}\right) \quad (14)$$

and

$$\hat{S}_{v_2}(f) \approx 3 \times 10^{-16}\,\mathrm{V}^2\,\mathrm{Hz}^{-1} \times \left(1 + \frac{20\,\mathrm{Hz}}{f}\right), \quad (15)$$

from which, taking into account that $M = 250$, $u(\hat{S}_{12}(f)) \approx 1.5 \times 10^{-17}\,\mathrm{V}^2\,\mathrm{Hz}^{-1}$ in the white noise region and $u(\hat{S}_{12}(f)) \approx 3 \times 10^{-16}\,\mathrm{V}^2/f$ in the $1/f$ noise region. A similar analysis can be performed for figure 7(b). Indeed, the type A uncertainty can be further reduced by increasing M.

To give a further example, we report in figure 8(a) a number of measurements on the sample AEM22A, in 2-terminal configuration at bias current levels of approximately 120 nA, 240 nA, 360 nA and 480 nA. Also in this case the rejection of uncorrelated noise is successful for all the spectra. It can be observed that the flicker noise level increases with the bias current. The expected quadratic dependence [42, 43] is confirmed by figure 8(b), which reports the spectra normalized to the square of the corresponding applied current.

We finally remark the virtual absence of 50 Hz power-line disturbances from the spectra of figures 7(a) and 7(b), showing the effectiveness of the shielding arrangement employed in the experiment (in figure 8(a), the level of 50 Hz disturbances is slightly higher because, at the time of that measurement, the grounding scheme was not yet optimized).

5. Conclusions

The spectrum analyzer described, based on digital sampling and a cross-correlation algorithm, allows measurements of excess noise at frequencies down to the 100 mHz range, limited only by the cutoff frequency

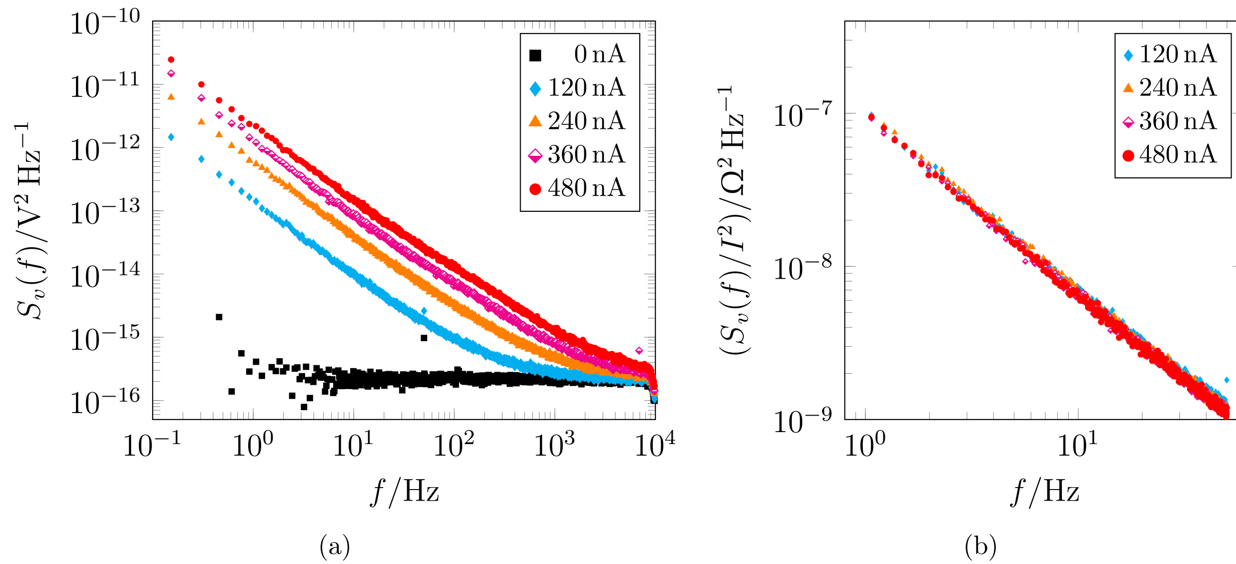

Figure 8: Voltage noise spectra of sample AEM22A at different bias current levels I in 2-terminal configuration (a). The same spectra were normalized to the corresponding bias current levels and their low frequency parts are shown in (b).

of the high-pass filters employed. The whole sequence of samples is recorded for off-line processing, allowing further statistical analyses to be performed, or the selective removal of outliers generated by burst interferences.

A model of the residual correlation effects, which can give rise to systematic noise errors, has been developed. The model and the experiment confirm that, whereas the employed general-purpose front-end amplifiers have a large flicker noise voltage, the resulting analyzer noise floor is white even at very low frequency.

Excess noise spectra from graphene samples, either in 2-terminal or 4-terminal configuration and at different bias current levels, were measured. The noise generated by a graphene layer and by the graphene-metal contacts was measured with high resolution, allowing accurate quantitative determinations of the flicker noise exponent, and of its magnitude dependence on the excitation current. These parameters are of special interest for the proper identification of the noise generation mechanisms as shown in [17].

Acknowledgments

The work has been realized within the Joint Resarch Project 16NRM01 GRACE: Developing electrical characterisation methods for future graphene electronics. This project has received funding from the EMPIR programme co-financed by the Participating States and from the European Union's Horizon 2020 research and innovation programme.

Bibliography

[1] H. Xu, L. Huang, Z. Zhang, B. Chen, H. Zhong, and L.-M. Peng, "Flicker noise and magnetic resolution of graphene Hall sensors at low frequency," *Appl. Phys. Lett.*, vol. 103, no. 11, p. 112405, 2013.

[2] S. Grover, S. Dubey, J. P. Mathew, and M. M. Deshmukh, "Limits on the bolometric response of graphene due to flicker noise," *Appl. Phys. Lett.*, vol. 106, no. 5, p. 051113, 2015.

[3] T. Wang, D. Huang, Z. Yang, S. Xu, G. He, X. Li, N. Hu, G. Yin, D. He, and L. Zhang, "A review on graphene-based gas/vapor sensors with unique properties and potential applications," *Nano-Micro Letters*, vol. 8, no. 2, pp. 95–119, Apr 2016. [Online]. Available: https://doi.org/10.1007/s40820-015-0073-1

[4] S. El-Ahmar, W. Koczorowski, A. A. Poźniak, P. Kuświk, W. Strupiński, and R. Czajka, "Graphene-based magnetoresistance device utilizing strip pattern geometry," *Appl. Phys. Lett.*, vol. 110, no. 4, p. 043503, 2017.

[5] M. Z. Hossain, S. Rumyantsev, M. S. Shur, and A. A. Balandin, "Reduction of $1/f$ noise in graphene after electron-beam irradiation," *Appl. Phys. Lett.*, vol. 102, no. 15, p. 153512, 2013.

[6] L. Huang, Z. Zhang, B. Chen, X. Ma, H. Zhong, and L.-M. Peng, "Ultra-sensitive graphene Hall elements," *Appl. Phys. Lett.*, vol. 104, no. 18, p. 183106, 2014.

[7] K. R. Amin and A. Bid, "High-performance sensors based on resistance fluctuations of single-layer-graphene transistors," *ACS Applied Materials & Interfaces*, vol. 7, no. 35, pp. 19 825–19 830, 2015.

[8] S. Rumyantsev, G. Liu, M. S. Shur, R. A. Potyrailo, and A. A. Balandin, "Selective gas sensing with a single pristine graphene transistor," *Nano letters*, vol. 12, no. 5, pp. 2294–2298, 2012.

[9] S. Rumyantsev, G. Liu, R. A. Potyrailo, A. A. Balandin, and M. S. Shur, "Selective sensing of individual gases using graphene devices," *IEEE Sensors Journal*, vol. 13, no. 8, pp. 2818–2822, 2013.

[10] R. Samnakay, C. Jiang, S. Rumyantsev, M. Shur, and A. Balandin, "Selective chemical vapor sensing with few-layer mos2 thin-film transistors: Comparison with graphene devices," *Applied Physics Letters*, vol. 106, no. 2, p. 023115, 2015.

[11] J. Lu, J. Pan, S.-S. Yeh, H. Zhang, Y. Zheng, Q. Chen, Z. Wang, B. Zhang, J.-J. Lin, and P. Sheng, "Negative correlation between charge carrier density and mobility fluctuations in graphene," *Phys. Rev. B*, vol. 90, no. 8, p. 085434, 2014.

[12] A. A. Balandin, "Low-frequency $1/f$ noise in graphene devices," *Nature Nanotech.*, vol. 8, no. 8, pp. 549–555, 2013.

[13] K. R. Amin and A. Bid, "Effect of ambient on the resistance fluctuations of graphene," *Appl. Phys. Lett.*, vol. 106, no. 18, p. 183105, 2015.

[14] H. N. Arnold, V. K. Sangwan, S. W. Schmucker, C. D. Cress, K. A. Luck, A. L. Friedman, J. T. Robinson, T. J. Marks, and M. C. Hersam, "Reducing flicker noise in chemical vapor deposition graphene field-effect transistors," *Applied Physics Letters*, vol. 108, no. 7, p. 073108, 2016. [Online]. Available: https://doi.org/10.1063/1.4942468

[15] S. L. Rumyantsev, M. S. Shur, G. Liu, and A. A. Balandin, "Low frequency noise in 2D materials: Graphene and MoS2," in *Noise and Fluctuations (ICNF), 2017 International Conference on*, June 2017, pp. 1–4.

[16] V. Kochat, C. S. Tiwary, T. Biswas, G. Ramalingam, K. Hsieh, K. Chattopadhyay, S. Raghavan, M. Jain, and A. Ghosh, "Magnitude and origin of electrical noise at individual grain boundaries in graphene," *Nano Letters*, vol. 16, no. 1, pp. 562–567, 2016, pMID: 26632989. [Online]. Available: https://doi.org/10.1021/acs.nanolett.5b04234

[17] A. Cultrera, L. Callegaro, M. Marzano, M. Ortolano, and G. Amato, "Role of plasma-induced defects in the generation of $1/f$ noise in graphene," *Applied Physics Letters*, vol. 112, no. 9, p. 093504, 2018. [Online]. Available: https://doi.org/10.1063/1.5024218

[18] M. J. Buckingham, *Noise in electronic devices and systems*. Horwood, 1985.

[19] E. Rubiola, C. Francese, and A. D. Marchi, "Long-term behavior of operational amplifiers," *IEEE Trans. Instrum. Meas.*, vol. 50, pp. 89–94, 2001.

[20] S. S. Martin, "Method and apparatus for measuring electrical noise in devices," US Patent 5 970 429, 1999.

[21] A. Blaum, O. Pilloud, G. Scalea, J. Victory, and F. Sischka, "A new robust on-wafer 1/f noise measurement and characterization system," in *Proceedings of the 2001 International Conference on Microelectronic Test Structures (ICMTS 2001)*, 2001.

[22] G. Giusi, O. Giordano, G. Scandurra, C. Ciofi, M. Rapisarda, and S. Calvi, "Automatic measurement system for the DC and low-f noise characterization of FETs at wafer level," in *Proceedings of the 2015 IEEE International Instrumentation and Measurement Technology*

Conference (I2MTC), may 2015.

[23] R. F. Voss and J. Clarke, "Flicker (1/f) noise: Equilibrium temperature and resistance fluctuations," *Phys. Rev. B*, vol. 13, pp. 556–573, 1976.

[24] M. Macucci and B. Pellegrini, "Very sensitive measurement method of electron devices current noise," *IEEE Trans. Instrum. Meas.*, vol. 40, pp. 7–12, 1991.

[25] "Stanford Research Systems SR785 — 100 kHz two-channel dynamic signal analyzer. Data sheet." [Online]. Available: https://www.thinksrs.com/products/sr785.html

[26] E. Rubiola, "The magic of cross correlation in measurements from dc to optics," in *Proc. 22nd European Frequency and Time Forum*, Toulouse, France, 22-25 April 2008.

[27] D. R. White, R. Galleano, A. Actis, H. Brixy, M. D. Groot, J. Dubbeldam, A. L. Reesink, F. Edler, H. Sakurai, R. L. Shepard, and J. C. Gallop, "The status of Johnson noise thermometry," *Metrologia*, vol. 33, no. 4, p. 325, 1996. [Online]. Available: http://stacks.iop.org/0026-1394/33/i=4/a=6

[28] H. J. Fink, "A new absolute noise thermometer at low temperatures," *Canadian Journal of Physics*, vol. 37, no. 12, pp. 1397–1406, 1959.

[29] J. J. Brophy, M. Epstein, and S. L. Webb, "Correlator-amplifier for very low level signals," *Review of Scientific Instruments*, vol. 36, no. 12, pp. 1803–1806, 1965.

[30] M. Sampietro, L. Fasoli, and G. Ferrari, "Spectrum analyzer with noise reduction by cross-correlation technique on two channels," *Review of scientific instruments*, vol. 70, no. 5, pp. 2520–2525, 1999.

[31] G. Ferrari and M. Sampietro, "Correlation spectrum analyzer for direct measurement of device current noise," *Review of scientific instruments*, vol. 73, no. 7, pp. 2717–2723, 2002.

[32] L. Callegaro, V. D'Elia, M. Pisani, and A. Pollarolo, "A Johnson noise thermometer with traceability to electrical standards," *Metrologia*, vol. 46, no. 5, p. 409, 2009.

[33] N. E. Flowers-Jacobs, A. Pollarolo, A. Weiss, K. Coakley, A. E. Fox, H. Rogalla, W. L. Tew, and S. P. Benz, "The NIST Johnson noise thermometry system for the determination of the Boltzmann constant," *J. Res. Natl. Inst. Stand. Technol.*, vol. 122, no. 46, 2017.

[34] N. E. Flowers-Jacobs, A. Pollarolo, K. J. Coakley, A. E. Fox, H. Rogalla, W. L. Tew, and S. P. Benz, "A Boltzmann constant determination based on Johnson noise thermometry," *Metrologia*, vol. 54, no. 5, p. 730, 2017. [Online]. Available: http://stacks.iop.org/0026-1394/54/i=5/a=730

[35] D. R. White, "Systematic errors in a high-accuracy Johnson noise thermometer," *Metrologia*, vol. 20, no. 1, p. 1, 1984. [Online]. Available: http://stacks.iop.org/0026-1394/20/i=1/a=002

[36] D. R. White and E. Zimmermann, "Preamplifier limitations on the accuracy of Johnson noise thermometers," *Metrologia*, vol. 37, no. 1, p. 11, 2000. [Online]. Available: http://stacks.iop.org/0026-1394/37/i=1/a=3

[37] L. Callegaro, M. Pisani, and M. Ortolano, "Systematic errors in the correlation method for Johnson noise thermometry: residual correlations due to amplifiers," *Metrologia*, vol. 47, no. 3, p. 272, 2010.

[38] "Keysight 35670A FFT dynamic signal analyzer, DC-102.4 kHz. Data sheet."

[39] M. B. Priestley, *Spectral analysis and time series*. Academic Press London, New York, 1981, vol. 2.

[40] ——, *Spectral analysis and time series*. Academic Press London, New York, 1981, vol. 1.

[41] D. R. White, S. P. Benz, J. R. Labenski, S. W. Nam, J. F. Qu, H. Rogalla, and W. L. Tew, "Measurement time and statistics for a noise thermometer with a synthetic-noise reference," *Metrologia*, vol. 45, pp. 395–405, 2008.

[42] F. N. Hooge, "$1/f$ noise," *Physica B+C*, vol. 83, pp. 14–23, 1976.

[43] L. K. J. Vandamme, "How useful is Hooge's empirical relation," in *2013 International Conference on Noise and Fluctuations (ICNF)*. IEEE, Jun. 2013.